The Astrophysical Journal, 905:168 (11pp), 2020 December 20 https://doi.org/10.3847/1538-4357/abcafe

Formation of Chromospheric Spicules in Magnetic Bright Points: An Analytical Approach Using Cartesian Slab Geometry

William Oxley[1], Joseph Scalisi[1], Michael S. Ruderman[1,2], and Róbert Erdélyi[1,3,4]
[1] Solar Physics and Space Plasma Research Centre, School of Mathematics and Statistics, University of Sheffield, Hicks Building, Hounsfield Road Sheffield, S3 7RH, UK; robertus@sheffield.ac.uk
[2] Space Research Institute (IKI) Russian Academy of Sciences, Moscow, Russia
[3] Department of Astronomy, Eötvös Loránd University, 1/A Pázmány Péter sétány, H-1117, Budapest, Hungary
[4] Gyula Bay Zoltań Solar Observatory (GSO), Hungarian Solar Physics Foundation (HSPF), Petőfi tér 3., Gyula, H-5700, Hungary
Received 2020 August 10; revised 2020 November 3; accepted 2020 November 15; published 2020 December 28

Abstract

We aim to provide insight into chromospheric spicules by suggesting a new formation mechanism. A magnetic field boundary condition is imposed, generating an Alfvén wave that shears a magnetic slab and propagates up the slab. The resulting Lorentz force accelerates material vertically, potentially nonlinearly driving a jet-like feature. This formation mechanism is applied to take place in a magnetic bright point embedded in the photosphere, providing motivation to use the simplifying assumption of a zero-β plasma. After deriving an analytical expression describing the vertical mass flux that constitutes the spicular jet, further understanding is gained by examining a model example of a magnetic field boundary condition in terms of standard functions. By visualizing the vertical mass flux through 3D plots, we demonstrate that the jet properties capture the observed properties of chromospheric spicules during their formation. This vindicates the model and simplifying assumptions used. Although we do not provide insight into the full evolution of a spicule, we show that the role of Alfvén waves triggered by shear in fact could be a viable formation mechanism for at least some chromospheric spicules. Consequently, we provide a starting point for further studies of this formation mechanism, which will lead to a greater understanding of the vast variety of chromospheric jets.

Unified Astronomy Thesaurus concepts: Solar spicules (1525); Solar chromosphere (1479); Alfven waves (23); Solar photosphere (1518); Magnetohydrodynamics (1964); Solar physics (1476); The Sun (1693); Solar magnetic bright points (1984)

Supporting material: animation

1. Introduction

Many studies that investigate solar spicules refer to Secchi's pioneering observations from the late 19th century (e.g., Roberts 1945; Beckers 1968, 1972; Tsiropoula et al. 2012). More recently, both numerical and analytical modeling have been an active area of solar spicular physics research, see reviews by, e.g., Sterling (2000) and Tsiropoula et al. (2012). The cross-sectional dimensions of spicules are very close to the resolution of imaging (De Pontieu et al. 2007; Zaqarashvili & Erdélyi 2009), meaning their formation and internal structure are still not understood in great detail. Their high velocities and dynamic behavior mean that spicules have the capacity to transfer significant amounts of mass and momentum into the outer parts of the solar atmosphere. As a result, spicules are viable candidates for supplying the significant non-thermal heating of the lower solar atmosphere from chromosphere to corona (Athay & Holzer 1982; De Pontieu et al. 2011) and could contribute to the solar wind, the source of which is one of the most important unanswered questions in solar physics. It is therefore of great interest and importance to study and understand solar spicules.

Spicules take the form of jet-like features that travel from the photosphere, up through the chromosphere and toward the transition region and the lower solar corona. Heights of about 7–13 Mm, widths of approximately 0.3–1.5 Mm and lifetimes of roughly 1–10 minutes are given in a review by Sterling (2000). This same source also provides good estimates for the velocity of the upward flux of material, to be a few tens of kilometers per second (many other sources support these estimates for spicule properties, e.g., Beckers 1972; Zaqarashvili & Erdélyi 2009; Tsiropoula et al. 2012; Samanta et al. 2019; Aschwanden 2019, chapter 5). Some observations suggest that speeds can be even higher (e.g., Sterling et al. 2010 and Martínez-Sykora et al. 2017 give velocities up to 150 km s^{-1}), and both heights and widths can be smaller (e.g., widths of 0.2 Mm and heights of 5 Mm as in Sterling et al. 2010).

The relatively small sizes and timescales of spicules limit what can be observed with our current instrumentation. However, it is expected that the capabilities of the Daniel K. Inouye Solar Telescope will allow for more detailed observations and advancement in the understanding of spicules. Observations of various group structures formed due to the high number of spicules are discussed by Beckers (1972). The "wheat field" pattern is an example of a distribution that can have a width of roughly 140 Mm (Lippincott 1957), suggesting that despite their small size, spicules can have large-scale impacts on the solar environment.

The apparent ending of a spicule either takes the form of material falling back through the chromosphere toward the solar surface, or simply fading from view (Sterling 2000; De Pontieu et al. 2007; Samanta et al. 2019). However, most of the material must return to the solar surface as the total outward flux of mass that spicules produce is much higher than that of the solar wind (Sterling 2000). It has been suggested that these highly localized jets may be classified in at least two categories: either type I or type II, based on their timescales and velocities.

Although both types of jets share similar features, type II "spicules" have shorter lifetimes and accelerate material to higher speeds, making them much more dynamic (De Pontieu et al. 2007; Tsiropoula et al. 2012; Aschwanden 2019, chapter 5). It is conjectured that these latter rapid jets (also labeled rapid blue/red excursions—RBEs/RREs—on disk) are governed by magnetic reconnection, while the traditional Secchi-type of spicules, which are the subject of our current paper, may be driven by a number of different physical processes.

The first step to understanding spicules is to understand how they form. There are multiple formation mechanisms, as mentioned, that have already been suggested. These include:

1. Granular buffeting: Turbulent motion in granules can buffet the side of intense flux tubes, which causes "squeezing" and results in vertical motion of plasma. Plasma motion driven this way may be interpreted as a spicule (Roberts 1979). Hollweg (1982) provides a mathematical analysis of spicule generation by a train of shock waves, where the physical mechanism that initially sets up the system is not specified. The author of this study also suggested that granular buffeting may provide the initial impulse required for the mechanism to occur.
2. Magnetic reconnection: Magnetic field lines break and reconnect into lower energy configurations, releasing vast amounts of kinetic energy that may even power large-scale eruptions, e.g., solar flares (Innes et al. 1997). It is therefore natural to expect that magnetic reconnection can generate smaller-scale dynamic motions of plasma as well, and some studies suggest that the thinner, more rapid jets (i.e., type II) are formed by this mechanism (De Pontieu et al. 2007; Sterling et al. 2010; Tsiropoula et al. 2012). However, even slower and wider spicules may also be generated by reconnection (as shown by, e.g., Samanta et al. 2019).
3. Global solar acoustic modes. Lower atmospheric shocks may also gain energy from the global solar acoustic p-mode oscillations and can accelerate material to form spicules (De Pontieu et al. 2004). De Pontieu et al. (2007) and Tsiropoula et al. (2012) suggest that this formation mechanism is associated with spicules, especially those with speeds at the lower end of the spicule propagation spectrum. A numerical investigation of shock wave-driven jets is given by Heggland et al. (2007), with their results showing a number of matching similarities with observations.
4. Ion–neutral collisions. It was suggested by Haerendel (1992) that damping of Alfvén waves by ion–neutral collisions could create a drag force, causing material to be lifted. Using an analytical model, De Pontieu & Haerendel (1998) built on these ideas, concluding that a spicule could be formed and sustained through this mechanism. This formation process was studied further by both James & Erdélyi (2002) and James et al. (2003), who numerically solved the fully nonlinear, dissipative 1.5D magnetohydrodynamic (MHD) equations, where waves were generated through a continuous sinusoidal driver. Their conclusions were that although the simulations produce features resembling spicules, the dominant formation process is due to the shocks that appear as a consequence of the interaction of forward propagating and reflected waves. This led the authors to question whether the ion–neutral collision mechanism could contribute to the production of spicules. It was suggested by James et al. (2003) that this formation mechanism may contribute to the generation of spicules by heating the environment before another process takes over, as many previous spicule models have struggled with low temperatures. Further investigation was conducted by Martínez-Sykora et al. (2017) through 2.5D MHD simulations, and the ion–neutral collisions were found to be critical in the formation process of the spicules.

From a physical point of view, all the above formation mechanisms may be split into two distinct categories: wave-driven or reconnection-driven. Both mechanisms can produce localized solar jets with properties consistent with observations of some spicules, while there are also observations that rule out one of the mechanisms for certain spicules. Therefore, the question of spicule formation remains open and it is conjectured that a number of jet formation mechanisms may operate in the lower solar atmosphere.

Here, we note that the study by Hollweg (1971) has addressed a somewhat similar problem but with a different methodology. He employed a perturbation method under similar overall assumptions and discussed the velocity and density perturbations in an infinite plasma. We emphasize the differences between our study and that of Hollweg (1971), with our equilibrium system differing from theirs, along with the application of this method to a new context, that of solar spicules. As mentioned above, the study by Hollweg (1982), building on the work of Hollweg et al. (1982), suggests spicules may be formed by the propagation of nonlinear Alfvén waves in a gravitationally stratified atmosphere. The mechanism described in that work suggests that the propagating Alfvén waves lead to the formation of shocks in the chromosphere. As the shocks pass through the transition region, they cause perturbations in the velocity that may match some of the observed properties of spicules. Although we do not rule out here that this shock formation mechanism may play some role in spicule formation, we will show that Alfvén waves can lead to the formation of jets, and matching observed properties of spicules, *even without* the formation of shocks. We also emphasize that Hollweg (1982) provides a numerical analysis, whereas here we provide an analytical study; both methods are critical to understanding the phenomenon of solar spicules.

A more recent theoretical model for the formation of spicules was proposed by Goodman (2012), where the driving mechanism for the vertical acceleration of plasma is the Lorentz force. This is a popular mechanism for other astrophysical jets on a variety of scales (see, e.g., Shibata & Uchida 1985, 1986a, 1986b; Kudoh & Shibata 1997; Vlahakis & Königl 2001; Smith 2012, chapter 9). In the study by Goodman (2012), the current density is specified using space- and timescales closely related to type II "spicules," and the velocity of the plasma is derived using the momentum equation. Unfortunately, the author overlooked another important MHD equation, and the proposed solution does not even satisfy the induction equation. Consequently, the study by Goodman (2012) does not apply to an MHD system and is not a feasible model for the formation of solar spicules. Therefore the modeling has to be revisited and a self-consistent mathematical approach may be desired.

Here, we take inspiration from Goodman (2012) for the physical concepts, and Jess et al. (2009) for the observational

aspects, who observed torsional Aflvén waves in magnetic bright points (MBPs; see discussion of MBPs below). We now provide a new model for spicule formation, driven by a Lorentz force, which occurs due to the nonlinear presence of Alfvén waves. The Alfvén waves apply a shearing motion, causing material to be "dragged," as they progress along the field lines nonlinearly. Various other studies provide further motivation to conduct this investigation. For example, observational aspects of photospheric swirls were investigated by Liu et al. (2019), who provided evidence suggesting that swirls can generate Alfvén pulses. This aligns with the physical model presented here, and similar pulses could provide the required shearing motion to generate solar spicules. In addition to this, through MHD simulations, Matsumoto & Shibata (2010) investigated photospheric granular motions that generate Alfvén waves, and suggested they could contribute to the formation of spicules.

In Section 3, two mechanisms will be described where a Lorentz force causes vertical acceleration of material. The first is direct vertical acceleration, and the second comes from the horizontal component of the Lorentz force, which causes squeezing and consequently vertical mass flux. The second of these mechanisms is ruled out in the context investigated here due to the zero-β approximation. Similar concepts were investigated by Martínez-Sykora et al. (2011) through numerical simulations, and the authors concluded that squeezing of chromospheric material leads to a vertical pressure gradient which propels the spicule.

We approach the formation of spicules using the regular perturbation method applied to the MHD equations describing motion in a magnetic slab model. Both a magnetic field and velocity shear are applied at the base of the slab, leading to propagation of Alfvén waves and consequently a field-aligned nonlinear flux of mass. The driving magnetic and velocity fields are applied at first order in the perturbations, and the effects and formation of the jet-like features will be obtained at second order as a result of the Lorentz force, which has a nonzero field-aligned component. Under a wide range of forms of the shear, a jet-like feature that resembles a spicule may be formed.

In this work, here, only the formation mechanism will be considered, and the subsequent full evolution of the jet will not be addressed. This is largely because gravity, and therefore density stratification, are ignored. In order to consider the full evolution of the generated jet as a model for a spicule, gravity would need to be taken into account along with the back reaction of Alfvén waves. These would be effects of third-order perturbations and would complicate the calculations considerably, therefore, at this stage, such an analysis will not be included. The aim here is simply to demonstrate the viability of jet formation due to the presence of Alfvén waves in a structured MHD waveguide.

Spicules are observed to travel upward through the chromosphere, therefore they are likely be formed below, at or close to the photosphere. In particular, spicular jets are observed to emerge from regions close to MBPs (Suematsu et al. 1982, 1995). Here we model this process by considering these MBPs as a magnetic slab, which is a good model for elongated MBPs (see Berger et al. 1995 and Zsámberger et al. 2018). We assume no external magnetism and use the zero-β approximation in the slab to simplify the problem. The first of the simplifications is justified as there are significant reductions in the strength of the field when moving from inside to outside of the MBP. MBPs are observed in the intergranular lanes, with magnetic fields of kilogauss order, whereas the surrounding photosphere has field strengths of only a few Gauss (Keys et al. 2013; Liu et al. 2018).

To justify the use of the zero-β approximation, consider the study by Hewitt et al. (2014) who used 3D MHD simulations to investigate the plasma properties inside MBPs, and the results showed the plasma-β to be small. As an explicit example, consider the properties of MBP2 given in Figure A1 of that paper, at time 300 s. The plasma-β can be calculated simply as $\beta \approx 0.35$, suggesting that $\beta \ll 1$ is possible. A model of a photospheric MBP was given by Shelyag et al. (2010), where the Alfvén speed was greater than the sound speed inside the MBP, again suggesting β can be taken to be small. This matches the intuitive idea that the plasma-β must be small in an MBP due to their intense magnetic fields, coupled with their reduced kinetic pressure, which results in their eponymous brightness (Keys et al. 2013).

During the mathematical analysis, we find that the zero-β approximation removes any effects that the boundaries of the slab may have on the vertical mass flux. Consequently, we lose one of the two contributing mechanisms, which is the squeezing of the slab leading to vertical mass flux, as discussed in Section 3. We point out that this approximation may limit application, and therefore we cannot analyze this second mechanism aiding jet formation in the present model. However, the approximation highlights the simplicity of the suggested formation mechanism; the external forces on the slab are not necessary and a jet can be formed directly from the dragging of material as the Alfvén waves propagate vertically.

In Section 2, we present the mathematical analysis of the formation mechanism using small perturbations. By specifying a driving magnetic field that applies a shear to the slab, an equation for the mass flux along the direction of the field lines is derived. The magnetic field is driven for a finite time, and is then reduced to zero, in order to determine how such a driver pushes mass upward. We start the analysis with the model description, outline the mathematical consequences of the physical simplifications, and then proceed to derive the equations that demonstrate the characteristic properties of the jet. Next, in Section 3, the physical argument behind the jet formation process is investigated. Here, the outlined mathematical ideas are put into context by assuming the mechanism takes place in an MBP. In Section 4, in order to demonstrate the entire concept, a targeted example of an Alfvén pulse is given, and the resulting field-aligned (i.e., vertical) mass flux is calculated. Some illustrations of the mass flux are also provided to aid the reader. We conclude in Section 5, with a critical discussion of the results, address the limitations of our method, and outline where the analytical study of spicule modeling may go in the future.

2. Mathematical Analysis of the Formation Mechanism

In this section, the mathematical modeling of the formation of a jet-like structure is considered, before it is put into physical context in Section 3. Consider a three-dimensional inviscid plasma split into three regions in the x-direction and unbounded in the y-direction. Consider the shear to take place at $z = 0$, and assume the slab is infinite for $z > 0$. The internal region ($|x| \leqslant x_0$), referred to as "the slab," has a width in the x-direction of $2x_0$, as shown in Figure 1. Throughout this work, assume the subscript j takes the value $j = 0$ and $j = e$ for the

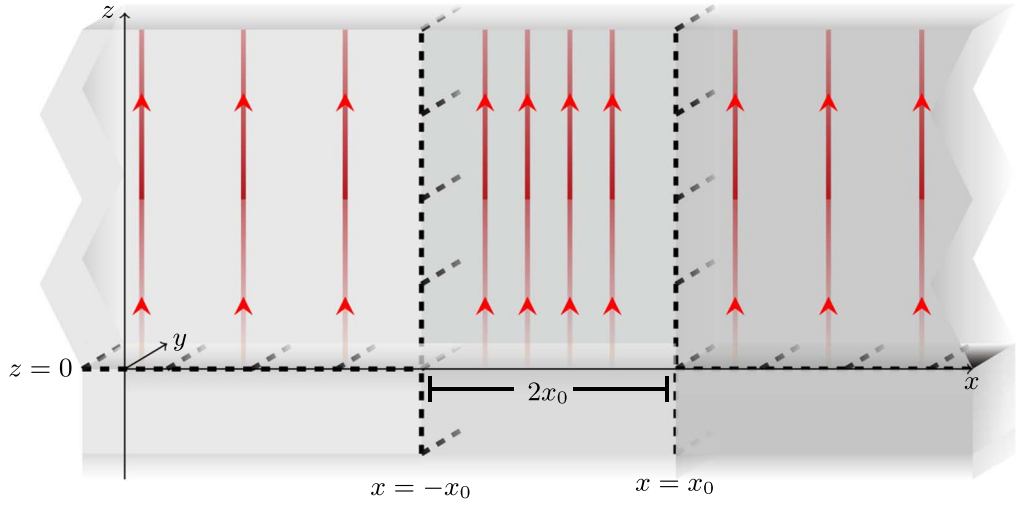

Figure 1. Visualization of the equilibrium magnetic slab. The magnetic field is indicated by the red lines.

internal and external regions, respectively. Assume the background equilibrium magnetic field is in the vertical (positive z) direction, and the background state in each region is homogeneous, with equilibrium pressure, temperature, density, and magnetic field strength given by p_j, T_j, ρ_j, and B_j, respectively. Define the Alfvén speed and sound speed in the region denoted by j as $v_{Aj}^2 = B_j^2/\rho_j\mu_0$ and $c_j^2 = \gamma p_j/\rho_j$, respectively, where μ_0 is the magnetic permeability of free space and γ is the adiabatic index. All quantities will be assumed independent of y in order to simplify the analysis. Consequently, instead of generating a jet that is finite in the y-direction, this mechanism will drive an infinite sheet of jet(s). To generate a jet which is localized in the y-direction we must consider a more general case. However, this would be a rather complex problem. Therefore, this general case will not be considered here. The simplifications of a zero-β plasma in the internal region and the removal of the external magnetic field will be made at a later stage, in order to find simple analytical results. These simplifications do limit the physics that the model can capture, however, the aim is merely to demonstrate that a jet (i.e., spicule mimicking lower solar atmospheric structuring) can be formed, and so this model is sufficient.

2.1. Driving the Jet

The regular perturbation method will be used to isolate the effect of propagation of Alfvén waves on jet formation. Consequently, a governing equation for the z (i.e., field-aligned, vertical) component of the velocity perturbation will be derived. This equation, then, has a simple relation to the vertical mass flux. Let ε be the ratio of the strength of the magnetic field perturbation to the strength of the background magnetic field, in the internal region. As we assume the perturbations are much smaller than the equilibrium quantities, we deduce that ε is a small parameter, and we assume the following functional form for all the variables in the problem:

$$f(x, z, t) = f_j + \sum_{i=1}^{\infty} f_i(x, z, t)\varepsilon^i. \tag{1}$$

Recall that for $|x| < x_0$, we have $j = 0$ and for $|x| > x_0$, $j = e$. The subscript j is only included for the equilibrium quantities, as these quantities depend on the region of x that is under consideration, but are locally constant within each given region. Using this subscript allows the equilibrium quantities to be written without x-dependence, and a solution to the problem can considered separately in each region. The functions f_i, which are the coefficients of the powers of ε in the summation of Equation (1), are written without the subscript j because they simply depend on x and so there is no need to identify more explicitly which region of x is under consideration for these functions.

Assume that there is no background bulk flow initially, giving $v_{xj} = v_{yj} = v_{zj} = 0$. The assumption that the background magnetic field is given by $\boldsymbol{B_j} = B_j\boldsymbol{e_z}$ gives $B_{xj} = B_{yj} = 0$. Additionally, since we know that the Alfvén waves decouple from the other wave perturbations in the currently employed geometry, we can isolate these waves by taking $p_1 = \rho_1 = v_{z1} = v_{x1} = B_{x1} = B_{z1} = 0$. The functional forms given in Equation (1) will be used to derive equations at each order of ε, up to and including second order. We therefore ignore terms of order ε^3 or smaller. We explicitly write the variables up to second order as

$$v_x = \varepsilon^2 v_{x2}, \quad v_y = \varepsilon v_{y1} + \varepsilon^2 v_{y2}, \quad v_z = \varepsilon^2 v_{z2}, \tag{2}$$

$$p = p_j + \varepsilon^2 p_2, \quad \rho = \rho_j + \varepsilon^2 \rho_2, \tag{3}$$

$$B_x = \varepsilon^2 B_{x2}, \quad B_y = \varepsilon B_{y1} + \varepsilon^2 B_{y2}, \quad B_z = B_j + \varepsilon^2 B_{z2}. \tag{4}$$

The ideal MHD equations are (see, e.g., Goedbloed & Poedts 2004, chapter 4)

$$\rho\frac{D\boldsymbol{v}}{Dt} = -\nabla p - \frac{1}{\mu_0}\boldsymbol{B} \times (\nabla \times \boldsymbol{B}), \tag{5}$$

$$\frac{\partial \rho}{\partial t} + \nabla \cdot (\rho \boldsymbol{v}) = 0, \tag{6}$$

$$\frac{D}{Dt}\left(\frac{p}{\rho^\gamma}\right) = 0, \tag{7}$$

$$\frac{\partial \boldsymbol{B}}{\partial t} = \nabla \times (\boldsymbol{v} \times \boldsymbol{B}), \quad \text{(along with } \boldsymbol{\nabla} \cdot \boldsymbol{B} = 0), \tag{8}$$

where ρ, p, $\boldsymbol{B}$, and $\boldsymbol{v}$ are the density, pressure, magnetic field, and velocity, respectively. The functional forms of the quantities given in Equations (2)–(4) will be substituted into

the ideal magnetohydrodynamic (MHD) equations, and equations at each order of perturbation will be obtained.

2.1.1. ε^0 Order

At ε^0 order the MHD equations are trivially satisfied. We require pressure balance across the boundaries in order for the equilibrium to be stable:

$$p_0 + \frac{B_0^2}{2\mu_0} = p_e + \frac{B_e^2}{2\mu_0}. \tag{9}$$

2.1.2. ε^1 Order

At ε^1 order, most of the equations are satisfied trivially, and the following relations can be derived for v_{y1} and B_{y1}:

$$\rho_j \frac{\partial v_{y1}}{\partial t} = \frac{B_j}{\mu_0}\frac{\partial B_{y1}}{\partial z}, \qquad \frac{\partial B_{y1}}{\partial t} = B_j \frac{\partial v_{y1}}{\partial z}. \tag{10}$$

Using these equations we can derive the wave equation for both v_{y1} and B_{y1},

$$\frac{\partial^2 v_{y1}}{\partial t^2} = v_{Aj}^2 \frac{\partial^2 v_{y1}}{\partial z^2}, \qquad \frac{\partial^2 B_{y1}}{\partial t^2} = v_{Aj}^2 \frac{\partial^2 B_{y1}}{\partial z^2}, \tag{11}$$

which have the well-known Alfvén wave solutions.

2.1.3. ε^2 Order

Using the ideal MHD equations, and collecting terms at ε^2 order gives the following set of equations:

$$\rho_j \frac{\partial v_{x2}}{\partial t} = -\frac{\partial p_2}{\partial x} - \frac{1}{\mu_0}\left(B_{y1}\frac{\partial B_{y1}}{\partial x} - B_j \frac{\partial B_{x2}}{\partial z} + B_j \frac{\partial B_{z2}}{\partial x}\right), \tag{12}$$

$$\rho_j \frac{\partial v_{y2}}{\partial t} = \frac{1}{\mu_0}\left(B_j \frac{\partial B_{y2}}{\partial z}\right), \tag{13}$$

$$\rho_j \frac{\partial v_{z2}}{\partial t} = -\frac{\partial p_2}{\partial z} - \frac{1}{\mu_0}\left(B_{y1}\frac{\partial B_{y1}}{\partial z}\right), \tag{14}$$

$$\frac{\partial \rho_2}{\partial t} + \rho_j \frac{\partial v_{x2}}{\partial x} + \rho_j \frac{\partial v_{z2}}{\partial z} = 0, \tag{15}$$

$$\frac{1}{p_j}\frac{\partial p_2}{\partial t} - \frac{\gamma}{\rho_j}\frac{\partial \rho_2}{\partial t} = 0, \tag{16}$$

$$\frac{\partial B_{x2}}{\partial t} = B_j \frac{\partial v_{x2}}{\partial z}, \tag{17}$$

$$\frac{\partial B_{y2}}{\partial t} = B_j \frac{\partial v_{y2}}{\partial z}, \tag{18}$$

$$\frac{\partial B_{z2}}{\partial t} = -B_j \frac{\partial v_{x2}}{\partial x}, \tag{19}$$

$$\frac{\partial B_{x2}}{\partial x} + \frac{\partial B_{z2}}{\partial z} = 0. \tag{20}$$

Note that Equation (20) is not strictly a governing equation but is derived from the solenoidal constraint.

We observe that Equations (13) and (18) decouple from the rest of the system, and as v_{y2} and B_{y2} are not the quantities of interest, we ignore these equations. By combining the remaining equations, one can derive fourth-order differential equations for the quantities v_{x2} and v_{z2}. Although we aim to find a solution for v_{z2}, the vertical velocity of plasma, it makes more sense to use the fourth-order differential equation for v_{x2} as boundary conditions at the interface of the slab need to be applied, and these boundary conditions will be in terms of v_{x2}. The governing differential equation for v_{x2} can be simplified using Fourier and Laplace transforms, and a solution for v_{x2} in Fourier/Laplace space can be found. Building on this, a relation is deduced then between v_{x2} and v_{z2} in this space, and the attention is focused on the vertical velocity v_{z2}. To find the solution from here in the real physical space, inverse Fourier and Laplace transforms are needed and difficulties arise due to poles of the counterpart of v_{z2} in Fourier/Laplace space. Due to these rather challenging mathematical difficulties, we leave this very cumbersome though rigorous and elegant approach for a later study (also discussed in Section 5). Instead, we simplify the system further using the zero-beta approximation. Here, we aim to simply demonstrate that this jet formation mechanism can exist, i.e., to make the point that Alfvén waves can drive the spicular jet formation, and so the simplification is justified.

Consider the internal region $-x_0 \leqslant x \leqslant x_0$, so that $j = 0$. The zero-β approximation provides the simplification that kinetic pressure is ignored. Consequently, $p_0 = 0$ and in this region $p_2 = 0$. Under the assumption that B_{y1} can be determined from the first-order equation, Equation (14) gives a simple equation for v_{z2},

$$\rho_0 \frac{\partial v_{z2}}{\partial t} = -\frac{1}{\mu_0}\left(B_{y1}\frac{\partial B_{y1}}{\partial z}\right). \tag{21}$$

2.2. Derivation of Mass Flux

2.2.1. Summary of Equations and Boundary Conditions

The equations that will be used for the solution are Equation (10), with $j = 0$ and Equation (21). It is easy to see from these equations that the solution for the vertical velocity, v_{z2}, in the internal region, is independent of the external region under the simplifications made here. For that reason, the rest of the analysis will only consider this internal region, i.e., we assume $x \in [-x_0, x_0]$ and $j = 0$.

In order to solve Equations (10) and (21) for v_{z2}, appropriate boundary or initial conditions must be imposed. Although a velocity shear may make more sense intuitively from a physical perspective, imposing a condition on B_{y1} is equivalent from an Alfvén wave perspective. It is pointed out by Equation (27) that there is a simple relation between B_{y1} and v_{y1}, so it is easy to extract the intuitive idea of a velocity shear from the magnetic field shear. Consider the following:

1. Let B_{y1} be given at $z = 0$ by

$$B_{y1}(x, 0, t) = B^*(x, t) = \begin{cases} B_T^*(x, t), & 0 \leqslant t \leqslant T, \\ 0, & \text{otherwise.} \end{cases} \tag{22}$$

This means that the magnetic field is driven for a characteristic time T and then it is "switched off." Ensuring that B_{y1} and B^* will be continuous functions of t gives $B_T^*(x, 0) = B_T^*(x, T) = 0$. At this stage, we also assume that there is no external magnetic field, meaning $B_e = 0$ and for $|x| > x_0$ we have $B_{y1} = 0$. To ensure that B_{y1} is continuous we then have $B^*(x_0, t) = B^*(-x_0, t) = 0$. This ensures that there are no magnetic forces applied to the slab from the external region.

2. The general solution for B_{y1} is a superposition of two counter-propagating waves, from Equation (10). Here, we ignore the wave that propagates in the negative z-direction, toward the subsurface regions of the Sun.
3. At $t = 0$, for all $z > 0$, assume $v_{z2} = 0$, i.e., there is initially no perturbed velocity in the z-direction.

2.2.2. Solution for B_{y1}

Consider the following Elsässer variables:

$$R_{\pm} = v_{y1} \pm \frac{v_{A0}}{B_0} B_{y1}, \tag{23}$$

then rearranging gives

$$v_{y1} = \frac{1}{2}(R_+ + R_-), \qquad B_{y1} = \frac{B_0}{2v_{A0}}(R_+ - R_-). \tag{24}$$

Now, by using Equation (10), differential equations for $R_{\pm}$ are found,

$$\frac{\partial R_+}{\partial t} = v_{A0}\frac{\partial R_+}{\partial z}, \qquad \frac{\partial R_-}{\partial t} = -v_{A0}\frac{\partial R_-}{\partial z}, \tag{25}$$

and the solutions are of the form

$$R_+ = R_+(t + z/v_{A0}), \qquad R_- = R_-(t - z/v_{A0}). \tag{26}$$

The condition that we ignore the wave that propagates backward from infinity (condition 2) immediately shows that $R_+ = 0$, and so Equation (24) gives

$$R_- = -\frac{2v_{A0}B_{y1}}{B_0}, \qquad v_{y1} = -\frac{v_{A0}B_{y1}}{B_0}. \tag{27}$$

The second of these equalities shows there is a simple relation between B_{y1} and v_{y1}. Equation (25) then gives a simple first-order differential equation for B_{y1},

$$\frac{\partial B_{y1}}{\partial t} = -v_{A0}\frac{\partial B_{y1}}{\partial z}. \tag{28}$$

Applying condition 1 above, given by Equation (22), the solution for B_{y1} takes a simple form,

$$B_{y1}(x, z, t) = B^*(x, t - z/v_{A0}) = \begin{cases} B_T^*(x, t - z/v_{A0}), & 0 \leqslant t - z/v_{A0} \leqslant T, \\ 0, & \text{otherwise.} \end{cases} \tag{29}$$

2.2.3. Solution for v_{z2}

Equation (21) is a simple differential equation for v_{z2}, and by applying the relation given by Equation (28) we find

$$\frac{\partial v_{z2}}{\partial t} = -\frac{1}{\rho_0\mu_0}\left(B_{y1}\frac{\partial B_{y1}}{\partial z}\right) = \frac{1}{\rho_0\mu_0 v_{A0}}\left(B_{y1}\frac{\partial B_{y1}}{\partial t}\right) = \frac{1}{2\rho_0\mu_0 v_{A0}}\left(\frac{\partial B_{y1}^2}{\partial t}\right). \tag{30}$$

Using the last equality and integrating with respect to t, the solution is found as follows:

$$v_{z2} = \frac{1}{2\rho_0\mu_0 v_{A0}} B_{y1}^2 + C(x, z), \tag{31}$$

where C is an arbitrary function of integration. Now, consider B_{y1} at $t = 0$ using Equation (29),

$$B_{y1}(x, z, 0) = B^*(x, -z/v_{A0}) = \begin{cases} B_T^*(x, -z/v_{A0}), & 0 \leqslant -z/v_{A0} \leqslant T, \\ 0, & \text{otherwise.} \end{cases} \tag{32}$$

Observe that for positive z, $-z/v_{A0} < 0$ and so $B_{y1}(x, z, 0) = 0$. Condition 3 also imposes that for positive z, $v_{z2}(x, z, 0) = 0$, and so using this in Equation (31) gives $C(x, z) = 0$.

Finally, substituting this result into Equation (31) along with Equation (29) gives the solution for v_{z2},

$$v_{z2} = \frac{1}{2\rho_0\mu_0 v_{A0}} B^{*2}(x, t - z/v_{A0}) = \begin{cases} \frac{1}{2\rho_0\mu_0 v_{A0}} B_T^{*2}(x, t - z/v_{A0}), & 0 \leqslant t - z/v_{A0} \leqslant T, \\ 0, & \text{otherwise.} \end{cases} \tag{33}$$

2.2.4. Field-aligned Mass Flux

The mass flux (or equivalently the momentum density) $\mathbf{\Phi}$ is defined as $\mathbf{\Phi} = \rho \boldsymbol{v}$, where ρ and $\boldsymbol{v}$ are the density and velocity of the plasma, respectively. Consider the z-component of $\mathbf{\Phi}$ in the same way as the other quantities using Equation (1). Using the form of ρ and v_z given by Equations (2) and (3) gives (recall that we use the equations with $j = 0$ corresponding to the internal region)

$$\Phi_z = (\rho_0 + \varepsilon^2\rho_2)(\varepsilon^2 v_{z2}) + O(\varepsilon^3) = \varepsilon^2\rho_0 v_{z2} + O(\varepsilon^3). \tag{34}$$

Now, define $\Phi = \rho_0 v_{z2}$, which is the leading component of the field-aligned (vertical) mass flux. Using Equation (33) we can simply write down the equation for Φ as

$$\Phi = \frac{1}{2\mu_0 v_{A0}} B^{*2}(x, t - z/v_{A0}) = \begin{cases} \frac{1}{2\mu_0 v_{A0}} B_T^{*2}(x, t - z/v_{A0}), & 0 \leqslant t - z/v_{A0} \leqslant T, \\ 0, & \text{otherwise.} \end{cases} \tag{35}$$

This solution for the vertical plasma flux shows that a jet-like feature can exist as a consequence of applying a shear perturbation to the base of the magnetic slab, which then propagates upward as dragged by an Alfvén wave. By specifying the initial magnetic field (B^*), it is now possible to capture some observational features of spicules, suggesting that this jet formation mechanism could be a viable and feasible source of solar spicules. An example will be given in Section 4 to demonstrate this.

3. Physical Description of the Formation Mechanism

Now that the mathematical formulation has been provided, the ideas will be put in the context of the solar photospheric

environment. In particular, we discuss the possibility of spicule formation in MBPs and elaborate on the physical process where the Lorentz force accelerates the plasma.

Consider the mathematical slab illustrated in Figure 1, and assume that this represents an MBP embedded in the photosphere. The physical idea here is that the formation occurs under conditions characteristic of an MBP, and then moves up through the chromosphere. Also, assume that the slab is aligned so that $z = 0$ is where the shear is applied and the formation mechanism begins. Recall that we only consider the formation mechanism, therefore we only consider photospheric conditions without accounting for a full evolution into the chromosphere.

Consider briefly the model that is introduced in Section 2, but for a slab of arbitrary internal plasma-β. Then, there are two processes that could both contribute to the material that is accelerated upward to cause the spicule generation. These are:

1. The direct acceleration of material in the vertical direction due to the vertical component of the Lorentz force.
2. The compression of the magnetic slab due to acceleration of material inward from the horizontal component of the Lorentz force (along with mass continuity).

However, due to the simplification that the internal region has $\beta = 0$, the second mechanism cannot contribute to the lifting of mass. This is easily observed through the calculations, as the z-component of the momentum equation is decoupled from the mass continuity equation (see Equations (14) and (15)). Consequently, the first mechanism is the focus of this study, and it is useful to break it down in more detail.

Recall that both the velocity and magnetic field perturbations (v_{y1} and B_{y1}) are driven through a boundary condition at $z = 0$, which relates to plasma motions that may occur in MBPs. In our model, the driver is active for a finite time T and is gradually reduced to zero. This boundary condition creates an Alfvén pulse that then propagates along the field lines into the higher regions of the chromosphere. The results suggest that a propagating Alfvén wave could cause the formation of a plasma jet by dragging material behind it.

The internal region has been assumed to be a zero-β plasma, and so the kinetic pressure is ignored. Consequently, examining Equation (5) shows that the z-component of the momentum equation has only one force, and this is the z-component of the Lorentz force $\boldsymbol{F} = \boldsymbol{j} \times \boldsymbol{B}$, where $\boldsymbol{B}$ is the magnetic field and $\boldsymbol{j} = (\boldsymbol{\nabla} \times \boldsymbol{B})/\mu_0$ is the current density. In the current approximation, the regular perturbation method has been used and a simple calculation shows $F_z = -\varepsilon^2 B_{y1}\partial_z B_{y1}/\mu_0 + O(\varepsilon^3)$. If the magnetic field is such that $F_z > 0$, then this mechanism can accelerate mass to generate and lift a plasma jet.

Now, consider the contribution of the magnetic tension and pressure forces separately. For the driver of the perturbations (i.e., ε-order), it is simple to show that the only force is the magnetic tension force. For the second-order perturbations in the field-aligned (vertical) direction (i.e., ε^2-order), both magnetic pressure and tension are nonzero. However, the magnetic tension force is canceled by part of the magnetic pressure. Consequently, the total force is the remaining pressure term.

The magnetic slab representing an MBP embedded in the photosphere has been illustrated in Figure 2, along with the driving boundary condition and Lorentz force. In this figure, the boundary magnetic field perturbation has been drawn to illustrate the shear that will be applied to the slab. If we wanted to consider a shear in the velocity field as opposed to the magnetic field, by using Equation (27) it is clear that in order to plot v_{y1} instead of B_{y1}, it would require a reversal of the blue arrows.

4. Example

In this section we present an example, where the boundary condition for the magnetic field B_{y1} is specified explicitly, and a jet-like feature is generated that captures the properties of a solar spicule.

The form of the boundary condition we consider here is

$$B_{y1}(x, 0, t) = \begin{cases} A\frac{|x|}{x}\sin^p\left(\pi\left[\frac{|x|}{x_0}\right]^q\right)\sin\left(\pi\frac{t}{T}\right), & 0 \leqslant t \leqslant T, \\ 0, & \text{otherwise}, \end{cases} \tag{36}$$

where A, p, q are positive constants. This is valid when $x \neq 0$. Define $B_{y1}(0, 0, t) = 0$, and observe that $B_{y1}(x, 0, t)$ is a continuous function of x at $x = 0$. Observe that this boundary magnetic field is a continuous function of t, which is localized and is a continuous function of x as it reduces to zero at the slab boundaries, where it meets the nonmagnetic region. It also applies a shear to the magnetic field in the x-direction.

4.1. Vertical Mass Flux

Using Equation (35), it is simple to write down the solution for the vertical mass flux Φ as follows:

$$\Phi = \rho_0 v_{z2} = \begin{cases} A'\sin^{2p}\left(\pi\left[\frac{|x|}{x_0}\right]^q\right)\sin^2\left(\pi\left[\frac{t}{T} - \frac{z}{Tv_{A0}}\right]\right), & 0 \leqslant \frac{t}{T} - \frac{z}{Tv_{A0}} \leqslant 1, \\ 0, & \text{otherwise}, \end{cases} \tag{37}$$

where $A' = A^2/2\mu_0 v_{A0}$. Figure 3 show the magnitude of Φ/A', as a function of non-dimensionalized variables x/x_0 and z/x_0, at times $t = 0.25T$, $0.5T$, and $0.75T$. The illustrations are produced in the region where z is positive and the solution is nonzero. For these plots, $q = 0.2$ and $p = 1.5$ are selected. The solution at time $t = 0$ is zero everywhere. After time $t = T$, it is simple to illustrate the solution as it is just a translation of the surface in Figure 3(d) in the positive z-direction. The speed of translation is v_{A0} and on the figure this corresponds to a translation of Tv_{A0}/x_0 for every characteristic time T, due to the non-dimensionalization of the variable z.

Figure 4 provides another visualization of the vertical mass flux, Φ, through a shaded contour map, at time $t = 0.5T$. The jet-like structure is observed clearly in this figure, and suggests that a recognizable jet feature is formed even after the driver has only been active for half of its lifetime. Note that for both Figures 3 and 4, the axis lengths have been chosen to qualitatively show that the jet is elongated in the z-direction. This comes from the small ratio of the slab width (which we consider to be the width of the MBP) to the vertical extent of the spicule, which is deduced through observations.

From the illustrations, it is evident that there is a localization of the upward mass flux, which propagates upward as time advances, perhaps resembling a spicule. Observations suggest that spicules can have widths as small as 0.2 Mm (Sterling et al. 2010),

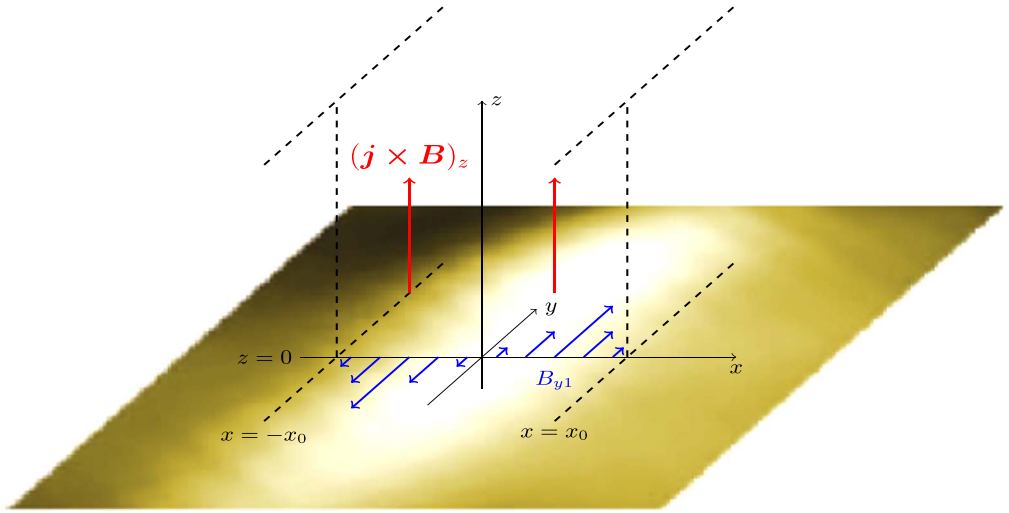

Figure 2. Illustration of the perturbations inside an MBP, which is represented by a magnetic slab, at time t with $0 < t < T$. The blue arrows visualize the magnetic field boundary condition applied at ε order through B_{y1}. The red arrows show the z-component of the Lorentz force. There are no labels on the y-axis on this illustration as the modeling is independent of y. The image of the MBP is adapted from Figure 12 of Liu et al. (2018).

and MBPs can have widths as large as 0.6 Mm (Berger et al. 1995). Consequently, it is reasonable to expect spicules to fill about half of the MBP width. This model matches these expectations, as when the jet-like feature is fully formed, it fills about half of the magnetic slab (see Figure 3(d)).

The model also suggests that there could be an absence of accelerated material in the center of the slab. Unfortunately, spicules have sizes very close to the observational spatial resolution limit (De Pontieu et al. 2007; Zaqarashvili & Erdélyi 2009), and so measuring the properties of spicules is a challenge. Detecting whether the upward accelerated material is present all the way to the center would be almost impossible as the estimated size of this center is much smaller than the size of the spicule, and consequently not detectable through observations at the moment.

Next, consider an Alfvén speed of around 10 km s^{-1} inside the MBP, which is an estimate based on the magnetic fields and densities given by Hewitt et al. (2014), who studied the evolution of plasma properties in MBPs through simulations (in particular, take the properties of the studied MBP given in Figure 1, at time $t = 300$ s). Assume the magnetic field boundary condition is driven for around 8 minutes (specifically, take $T = 500$ s). By inspecting Figure 3(d), we see that when the jet has fully formed, its vertical field-aligned extent is 1 unit of Tv_{A0}. Consequently, we deduce the vertical extent of this feature to be $\approx$5 Mm. This matches well with the length of some spicules (Sterling et al. 2010), once again suggesting our model is consistent with observations.

A comparison between the vertical extent suggested by this model and the spicule heights found in observations may not be appropriate as the model only considers the formation of the jet and not its subsequent evolution. This is because, as the jet moves into the chromosphere, its longitudinal extent may evolve due to gravitational effects before it can be observed. However, we do gain an indication that this mechanism is viable to generate jets with the dimensions consistent with observations. Note that the driving time, T, has a direct relation with the vertical extent and can be constrained in order to generate a length that agrees with observations. We should ensure that the driving time is of the correct order of magnitude, and by comparing to the lifetime of jets, specifying it to be a few minutes is reasonable (Sterling 2000).

Recall that the mass flux in the field-aligned z-direction, as discussed in Section 2, is actually $\Phi_z = \varepsilon^2\Phi$, where ε is the small parameter used in the perturbation method. This small parameter would have to be taken into account when analyzing the amplitude of the mass flux. However, it will not impact the extent of the feature, as in this model it simply translates vertically at speed v_{A0}. Even though the amplitude of the mass flux is small due to the ε^2 factor, the mass flux may still be consistent with chromospheric spicules. This is a consequence of the stratification of the solar atmosphere; due to the extreme changes in the density as height above the photosphere is increased (Haerendel 1992), a small amount of material accelerated from the photosphere would be significant when it reached the chromosphere.

5. Discussion

The generation of spicules is still an unsolved and challenging problem in solar physics, in spite of the highly important momentum and energy transfer capabilities of these localized jets. In this work we revisited some of the ideas presented by Goodman (2012) and built on the premise that a spicule may be formed due to the Lorentz force, providing a novel self-consistent analytical study of the concept.

By considering a perturbation theory approach, this work demonstrates that some of the key properties of chromospheric jet-like features (with applications to spicules) can be obtained as a consequence of Alfvén waves, which apply a shear to the magnetic waveguide, a slab in this case. The resulting upward flux of mass turns out to be a direct consequence of the field-aligned propagating Alfvén waves, which drag material vertically. Because of this, we reemphasize that shock formation is not needed to cause the jet, meaning the process here is different to that studied by Hollweg (1971). The formation mechanism described here is particularly applicable to MBPs, where spicules are observed to emerge from (Suematsu et al. 1982, 1995). The proposed mechanism is put into the context of an MBP embedded in the photosphere,

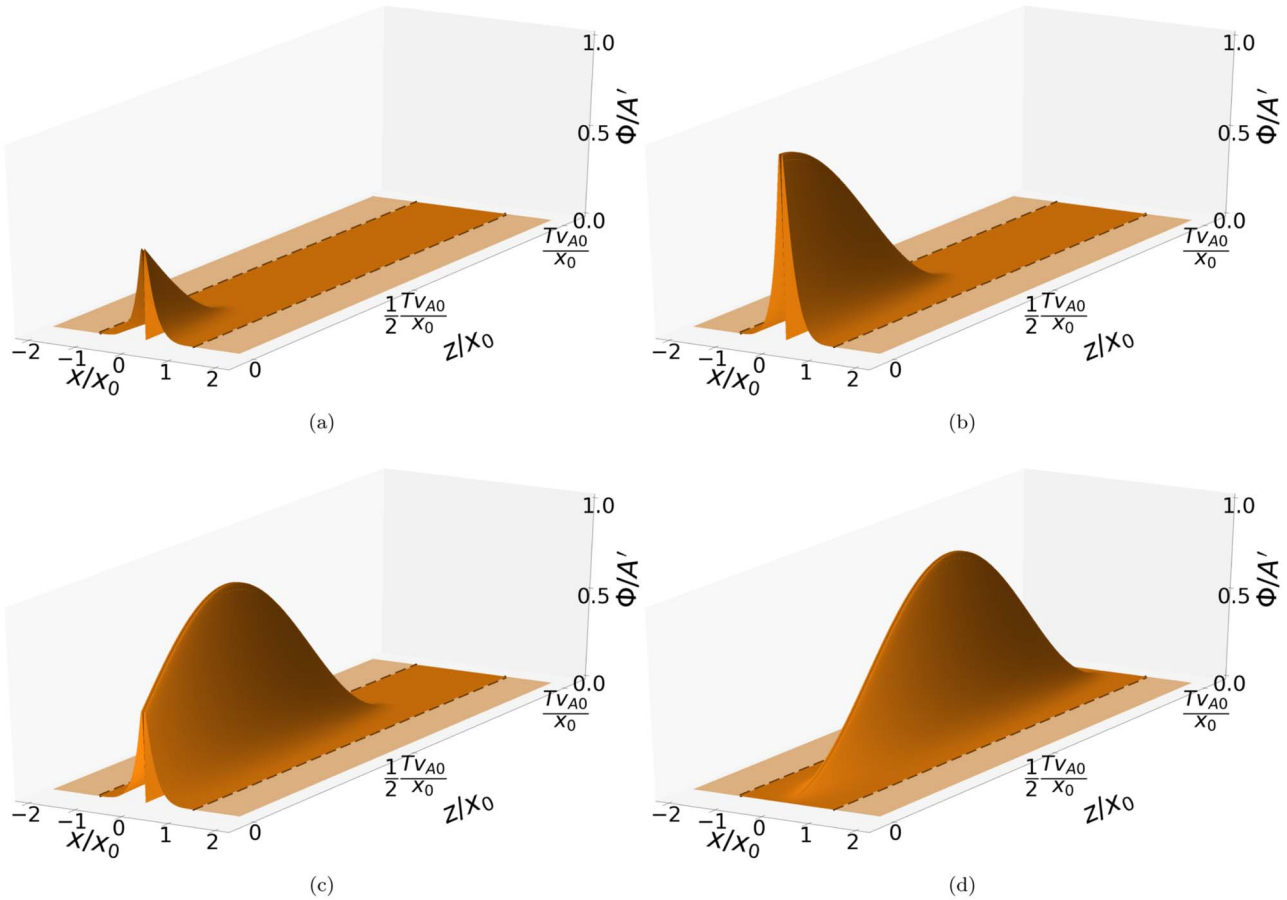

Figure 3. Illustrations showing Φ/A' given by Equation (37) (with $q = 0.2$ and $p = 1.5$) for various x and z at times (a) $t = 0.25T$, (b) $t = 0.5T$, (c) $t = 0.75T$ and (d) $t = T$. The dashed black lines represent the interfaces at the edge of the slab. An animated version of this figure is available online. This is a 10 s clip showing Φ/A' between times $t = 0$ and $t = 2T$. The z/x_0 axis in the animation is doubled in length in order to observe the surface all the way through to $t = 2T$.

(An animation of this figure is available.)

and it is suggested that the formation process takes place here, after which the feature will travel up through the chromosphere.

Equations (33) and (35) give the velocity and mass flux, respectively, and immediately show that there is upward flux of plasma, which is indicative of a spicule. The equations reveal that the upward flux of plasma is a direct consequence of the magnetic field boundary condition. Due to the direction and spatial dependencies of the driving magnetic field, there is a nonzero component of the Lorentz force in the positive z-direction, and this is the force that accelerates plasma to drive the jet-like feature. Then, by specifying this boundary magnetic field to shear the slab, we have demonstrated through an arbitrary but appropriate example that the resulting Alfvén waves may indeed be the catalyst for jets of plasma to occur.

To make further comparisons to observed spicules, the form of the shearing magnetic field must be specified, ideally from observations. The working example presented in Section 4 may generate a jet-like feature that shares characteristic properties with spicules at their initial phase of evolution. Some discussion relating to observations reveals that there are good aspects to this model, capturing well what is observed for some spicules. Specifically, the jet-like feature is localized in the field-aligned vertical direction, and this localization moves vertically upward as time advances. This can be seen from Figure 3, along with the movie provided online. In addition, the jet fills half of the slab which, again, matches the expectations from observations (Berger et al. 1995; Sterling et al. 2010). The vertical extent of a spicule is a characterizing feature and has been estimated here and shown to be of the same order as observations. However, we emphasize that it is not suggested to directly compare the vertical extent in the model with that found in observations. This is because gravitational effects may change the longitudinal structure of the jet before observations are made in the chromosphere. Figure 4 provides an additional illustration to aid in the understanding of the presented ideas, and is a further qualitative indication that this formation process may generate jets resembling spicules. The figure illustrates the mass flux at only half of the characteristic time T, and suggests a recognizable jet-like feature can be produced, even before the driving shear has finished acting on the system.

5.1. Limitations

Unfortunately, there are some limitations of this method, and they should be discussed in order to critically assess why the model is still applicable. The assumption that there is no y-dependence in the modeling means that what is obtained is actually an infinite sheet of jet, as opposed to a localized one. To generate a finite jet, y-dependence would have to be addressed, and the analysis would be much more complicated. This is not a showstopper as we are still able to demonstrate that the proposed formation mechanism is viable and can produce a jet-like feature. A y-dependence may be addressed,

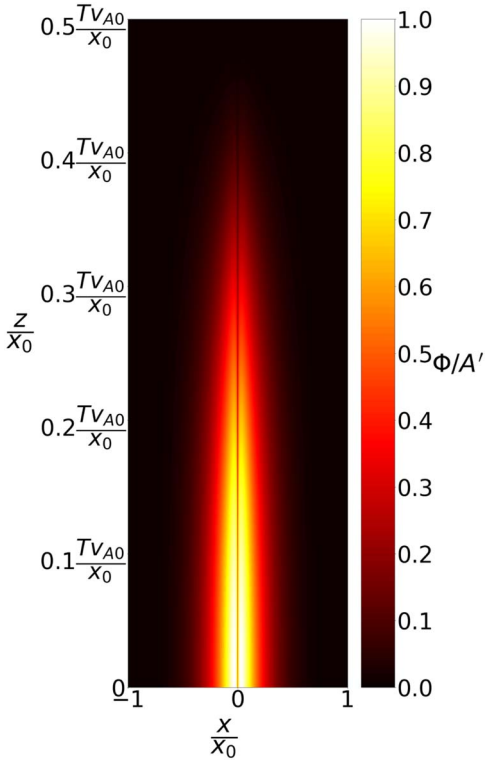

Figure 4. Illustration of Φ/A' in the x–z plane at time $t = 0.5T$. The colors show the magnitude of Φ/A' given by Equation (37) (with $q = 0.2$ and $p = 1.5$) as indicated in the color bar on the right-hand side of the figure.

e.g., by using the WKB-method that is cumbersome and is beyond the scope of the current study.

Figure 3 suggests that the jet has an evacuated central region, with the accelerated material not forming at $x = 0$. This could be an artifact of the actual model shear, and we may need to consider a more general case to overcome this issue. However, this is only a minor problem as spicules themselves are close to the spatial resolution of observations (De Pontieu et al. 2007; Zaqarashvili & Erdélyi 2009), and so the evacuated center would be too small to observe, meaning that our results still do not contradict observations of spicules.

The model here is only applicable to the initial formation phase of a jet, not to the subsequent full evolution. Consequently, we cannot gain insight into the jet as it travels up through the entire chromosphere. This limitation is most easily observed through Equation (35), which suggests the jet would translate toward infinity. If additional factors such as density stratification, variable temperature, and gravity were taken into account, along with the back reaction of Alfvén waves, it may be possible to model the full evolution of a spicule using the method outlined here. Considering such features in the modeling would complicate the analysis considerably, and the third-order perturbations would become important. Most importantly, it would lead to the jet having a limited lifetime and only reaching a finite height within the lower solar atmosphere, before falling back down to the photosphere due to gravitational stratification.

The limitations of the model discussed above could be used as an inspiration for a further study. Visualizing the height by time–distance techniques would provide interesting and potentially groundbreaking comparison to observations and numerical simulations, and the aim would be to capture the observed parabolic paths on these time–distance diagrams using the proposed model (De Pontieu et al. 2007; Heggland et al. 2007; Pereira et al. 2014).

5.2. Possibilities of Further Study

Let us now consider briefly the same formation mechanism, under the same assumptions, apart from the internal region has arbitrary plasma-β. Returning to Equations (12)–(19), a higher-order differential equation for v_{x2} could be derived. To solve this, we could apply Fourier and Laplace transforms to this equation. This should be then followed by applying kinematic and dynamic boundary conditions at $x = \pm x_0$. Then, using inverse Fourier and Laplace transforms, an equation for v_{z2} could be obtained and the vertical mass flux can be deduced, as discussed in Section 2. The key issue is the yet unknown way to resolve the mathematical challenge associated with the inverse Laplace transform of the leaky waves. This would not be a simple extension of the zero-β, and is therefore well beyond the scope of the current study. In this generalization, as well as the direct acceleration of material, another contribution to the jet formation would be present due to the x-component of the Lorentz force. More precisely, the inward accelerated plasma causes the slab to squeeze, consequently material is accelerated up the slab, in order to conserve mass (as discussed in Section 3).

Finally, an analog derivation could be made using cylindrical geometry, where the magnetic flux tube replaces the magnetic slab. Magnetic flux tubes are the fundamental building blocks for many solar features, with intense flux tubes responsible for the observed kilogauss magnetic fields (Ryutova 2015). Flux tubes are therefore the basic model building blocks for many analytical or numerical studies in solar physics (see, e.g., Roberts & Webb (1978) for an analytical wave study using the flux tube model). The assumption of axial symmetry about the vertical axis in the flux tube model is equivalent to the assumption of y-independence used in the magnetic slab model. An advantage of employing the flux tube model is that a single axially symmetric jet would be generated as opposed to the jet sheet found in the magnetic slab model. Conducting this study using both types of geometry allows us to apply the formation mechanism to a wider range of MBPs. As well as the elongated MBPs that are discussed in the context of the slab geometry, we can apply the formation mechanism using the magnetic flux tube model to the more circularly shaped MBPs (see Liu et al. 2018 for specific examples of observed MBPs, taking both elongated and circular shapes). Cylindrical geometry will be used in a follow-up study to illustrate the jet formation mechanism, building on the work presented here.

R.E. and M.S.R. are grateful to Science and Technology Facilities Council (STFC; grant No. ST/M000826/1) UK and the Royal Society for enabling this research. R.E. also acknowledges the support received by the CAS Presidents International Fellowship Initiative grant No. 2019VMA052 and the warm hospitality received at USTC of CAS, Hefei, where part of his contribution was made.

ORCID iDs

William Oxley https://orcid.org/0000-0001-7434-0292
Joseph Scalisi https://orcid.org/0000-0001-7070-6322
Michael S. Ruderman https://orcid.org/0000-0003-2324-8466
Róbert Erdélyi https://orcid.org/0000-0003-3439-4127

References

Aschwanden, M. J. 2019, New Millennium Solar Physics, Vol. 458 (Berlin: Springer)
Athay, R. G., & Holzer, T. E. 1982, ApJ, 255, 743
Beckers, J. M. 1968, SoPh, 3, 367
Beckers, J. M. 1972, ARA&A, 10, 73
Berger, T. E., Schrijver, C. J., Shine, R. A., et al. 1995, ApJ, 454, 531
De Pontieu, B., Erdélyi, R., & James, S. P. 2004, Natur, 430, 536
De Pontieu, B., & Haerendel, G. 1998, A&A, 338, 729
De Pontieu, B., McIntosh, S., Hansteen, V. H., et al. 2007, PASJ, 59, S655
De Pontieu, B., McIntosh, S. W., Carlsson, M., et al. 2011, Sci, 331, 55
Goedbloed, J. P. H., & Poedts, S. 2004, Principles of Magnetohydrodynamics (Cambridge: Cambridge Univ. Press)
Goodman, M. L. 2012, ApJ, 757, 188
Haerendel, G. 1992, Natur, 360, 241
Heggland, L., De Pontieu, B., & Hansteen, V. H. 2007, ApJ, 666, 1277
Hewitt, R. L., Shelyag, S., Mathioudakis, M., & Keenan, F. P. 2014, A&A, 565, A84
Hollweg, J. V. 1971, JGR, 76, 5155
Hollweg, J. V. 1982, ApJ, 257, 345
Hollweg, J. V., Jackson, S., & Galloway, D. 1982, SoPh, 75, 35
Innes, D. E., Inhester, B., Axford, W. I., & Wilhelm, K. 1997, Natur, 386, 811
James, S. P., & Erdélyi, R. 2002, A&A, 393, L11
James, S. P., Erdélyi, R., & De Pontieu, B. 2003, A&A, 406, 715
Jess, D. B., Mathioudakis, M., Erdélyi, R., et al. 2009, Sci, 323, 1582
Keys, P. H., Mathioudakis, M., Jess, D. B., et al. 2013, MNRAS, 428, 3220
Kudoh, T., & Shibata, K. 1997, ApJ, 474, 362
Lippincott, S. L. 1957, SCoA, 2, 15
Liu, J., Nelson, C. J., Snow, B., Wang, Y., & Erdélyi, R. 2019, NatCo, 10, 3504
Liu, Y., Xiang, Y., Erdélyi, R., et al. 2018, ApJ, 856, 17
Martínez-Sykora, J., De Pontieu, B., Hansteen, V. H., et al. 2017, Sci, 356, 1269
Martínez-Sykora, J., Hansteen, V., & Moreno-Insertis, F. 2011, ApJ, 736, 9
Matsumoto, T., & Shibata, K. 2010, ApJ, 710, 1857
Pereira, T. M. D., De Pontieu, B., Carlsson, M., et al. 2014, ApJL, 792, L15
Roberts, B. 1979, SoPh, 61, 23
Roberts, B., & Webb, A. R. 1978, SoPh, 56, 5
Roberts, W. O. 1945, ApJ, 101, 136
Ryutova, M. 2015, Physics of Magnetic Flux Tubes, Vol. 417 (Berlin: Springer)
Samanta, T., Tian, H., Yurchyshyn, V., et al. 2019, Sci, 366, 890
Shelyag, S., Mathioudakis, M., Keenan, F. P., & Jess, D. B. 2010, A&A, 515, A107
Shibata, K., & Uchida, Y. 1985, PASJ, 37, 31
Shibata, K., & Uchida, Y. 1986a, PASJ, 38, 631
Shibata, K., & Uchida, Y. 1986b, SoPh, 103, 299
Smith, M. D. 2012, Astrophysical Jets and Beams (Cambridge: Cambridge Univ. Press)
Sterling, A. C. 2000, SoPh, 196, 79
Sterling, A. C., Moore, R. L., & DeForest, C. E. 2010, ApJL, 714, L1
Suematsu, Y., Shibata, K., Neshikawa, T., & Kitai, R. 1982, SoPh, 75, 99
Suematsu, Y., Wang, H., & Zirin, H. 1995, ApJ, 450, 411
Tsiropoula, G., Tziotziou, K., Kontogiannis, I., et al. 2012, SSRv, 169, 181
Vlahakis, N., & Königl, A. 2001, ApJL, 563, L129
Zaqarashvili, T. V., & Erdélyi, R. 2009, SSRv, 149, 355
Zsámberger, N. K., Allcock, M., & Erdélyi, R. 2018, ApJ, 853, 136